

Multiatribute rotation scheme: A tool for reservoir property prediction from seismic inversion attributes

Pedro Alvarez¹, Francisco Bolívar¹, Mario Di Luca², and Trino Salinas²

Abstract

The multiatribute rotation scheme (MARS) is a methodology that uses a numerical solution to estimate a transform to predict petrophysical properties from elastic attributes. This is achieved by estimating a new attribute in the direction of maximum change of a target property in an n -dimensional Euclidean space formed by an n number of attributes and subsequent scaling of this attribute to the target unit properties. We have computed the transform from well-log-derived elastic attributes and petrophysical properties, and we have posteriorly applied it to seismically derived elastic attributes. Such transforms can be used to estimate reservoir property volumes for reservoir characterization and delineation in exploration and production settings and to estimate secondary variables in geostatistical workflows for static model generation and reserve estimation. To illustrate the methodology, we applied MARS to estimate a transform to predict the water saturation and total porosity from elastic attributes in a well located in the Barents Sea as well as to estimate a water-saturation volume in a mud-rich turbidite gas reservoir located onshore Colombia.

Introduction

A common way to understand the relationship between seismic attributes and a petrophysical property is by the use of rock-physics templates (Ødegaard and Avseth, 2004) or simply by cross plotting well-log-derived elastic attributes against a color-coded petrophysical property. Both ways graphically illustrate the relationship between the elastic and petrophysical domains, which can be used to estimate reservoir properties from seismic inversion attributes. The multiatribute rotation scheme (MARS) is a methodology that uses a numerical solution to estimate a mathematical expression that reproduces the aforementioned phenomena. This method uses measured and/or rock-physics-modeled well-log information, as an input, to estimate a well-log-derived transform between several elastic attributes and the target petrophysical properties. Multiple elastic attributes such as P-wave impedance I_P , S-wave impedance I_S , P-to-S velocity ratio V_P/V_S , the product of density and Lamé's parameters $\lambda\rho$ and $\mu\rho$ (Goodway et al., 1997), Poisson's ratio σ , the product of density by bulk modulus $K\rho$, the product of density and dynamic Young's modulus $E\rho$, Poisson dampening factor (PDF) (Mazumdar, 2007), elastic impedance (Connolly, 1999), PS elastic impedance (Gonzalez et al., 2003), etc., can be used in the MARS assessment. This methodology evaluates the relationship between all possible elastic attributes spaces

and a target petrophysical property using a similar correlation approach to the one used by Whitcombe et al. (2002) in the extended elastic impedance methodology. The final goal of this workflow is to apply the resultant transform over seismically derived elastic attributes to predict the spatial distribution of petrophysical reservoir properties.

Method and theory

MARS estimates a new attribute τ in the direction of maximum change of a target property in an n -dimensional Euclidean space formed by an n number of attributes. We search for the maximum correlation between the target property and all of the possible attributes that can be estimated via an axis rotation of the basis that forms the aforementioned space. Figure 1a shows a sketch illustrating an example for the particular case of two dimensions. This figure shows a crossplot of two attributes color coded by a target property. Dashed gray arrows represent new attributes estimated via axis rotation. The blue arrow represents the elastic attribute τ that shows the maximum correlation with the target petrophysical property. In Figure 1b, the angles of the rotation (θ) used to estimate the new set of attributes are crossplotted against its correlation coefficients with the target property, with the goal of identifying the angle exhibiting the maximum correlation (θ_i).

¹Rock Solid Images, Houston, Texas, USA. E-mail: pedro.alvarez@rocksolidimages.com; francisco.bolivar@rocksolidimages.com.

²Pacific Rubiales Energy, Bogota, Colombia. E-mail: mdiluca@pacificrubiales.com.co; tsalinas@pacificrubiales.com.co.

Manuscript received by the Editor 30 January 2015; revised manuscript received 17 April 2015; published online 24 July 2015. This paper appears in *Interpretation*, Vol. 3, No. 4 (November 2015); p. SAE9–SAE18, 10 FIGS., 1 TABLE.

<http://dx.doi.org/10.1190/INT-2015-0029.1>. © 2015 Society of Exploration Geophysicists and American Association of Petroleum Geologists. All rights reserved.

The attribute τ for the specific cases of two and three dimensions are given by

$$\tau = A_1 \times S_1 \times \sin(\theta_i) + A_2 \times S_2 \times \cos(\theta_i) \quad (1)$$

and

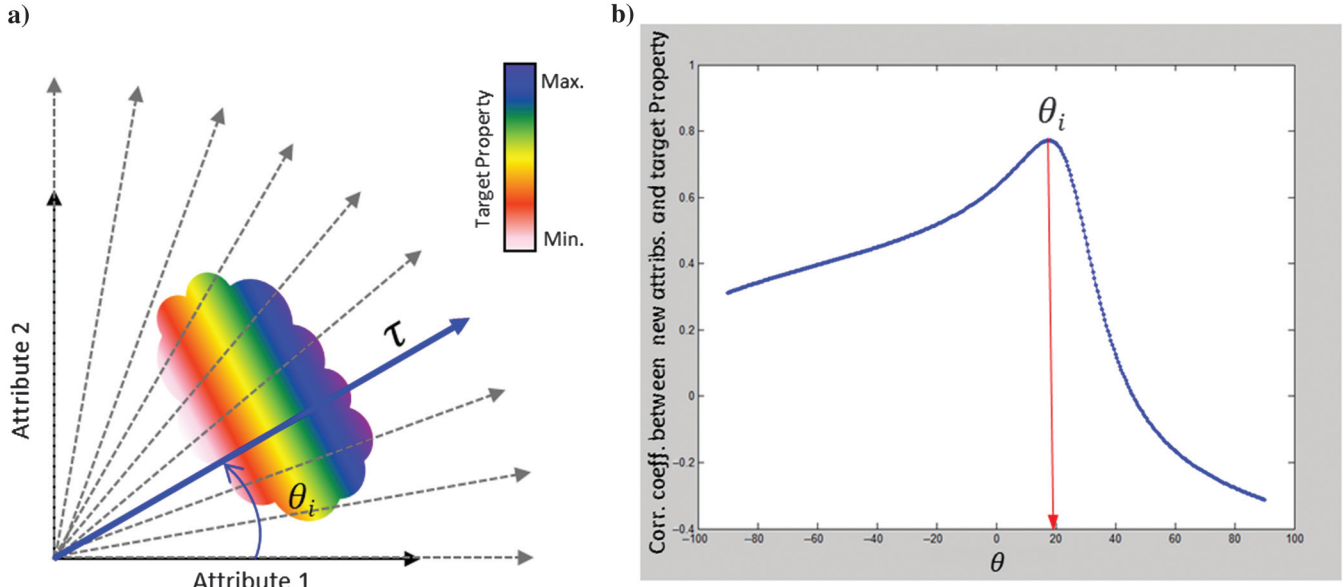


Figure 1. (a) Sketch of a crossplot of two attributes color coded by a target property. The dashed gray lines represent new attributes estimated via axis rotation, and the blue line represents the attribute that shows the maximum correlation coefficient with the target property. (b) Example of a crossplot between the angles of rotation and the correlation coefficients calculated at each of these angles.

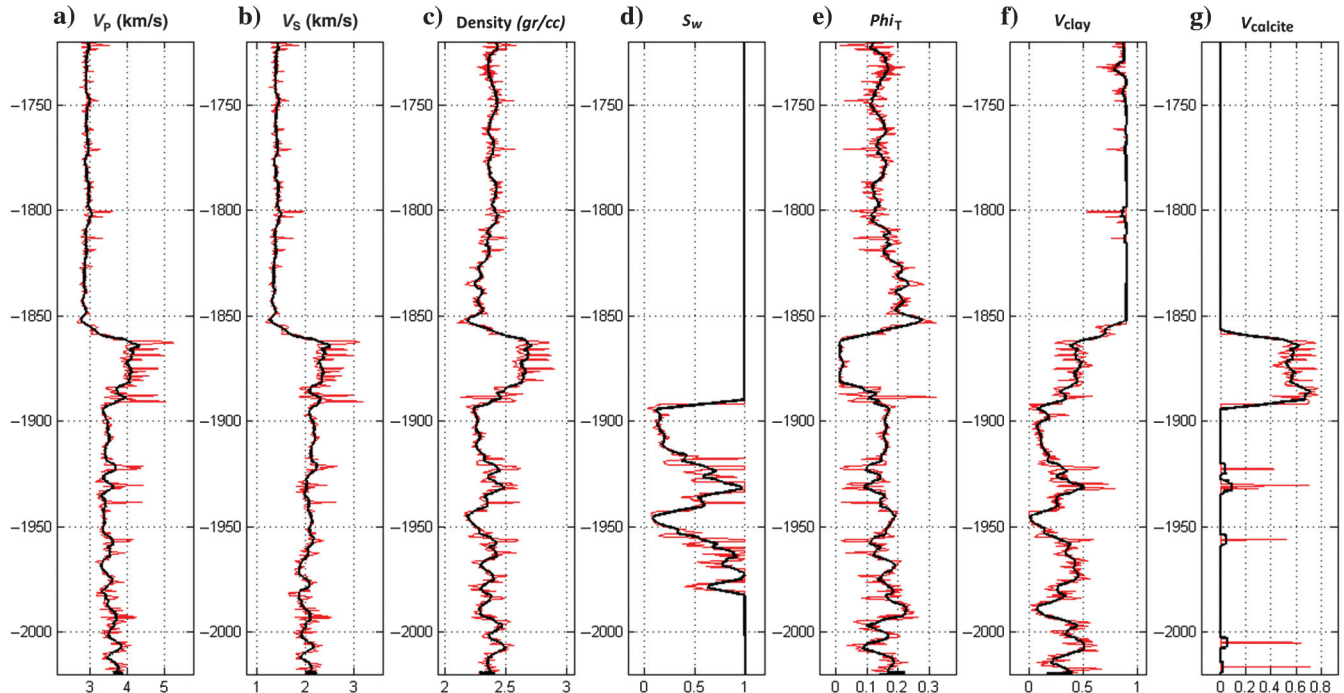


Figure 2. Panels (a-g) show V_p , V_s , density, S_w , ϕ_t , V_{clay} , and V_{calcite} . The red curves show the original logs, whereas the black curves show upscaled versions to seismic resolution, which were obtained by low-pass filtering the input well logs.

$$\begin{aligned} \tau &= (A_1 \times S_1 \times \sin \theta_i + A_2 \times S_2 \times \cos \theta_i) \times \sin \varphi_j \\ &+ A_3 \times S_3 \times \cos \varphi_j, \end{aligned} \quad (2)$$

the maximum correlation is reached (Figure 1b); and n is the number of input attributes. Using attributes with similar orders of magnitude is a necessary condition to achieve an effective evaluation of any attribute space because constant angle sampling is used in axis rotations. Because different attribute combinations produce different results, this methodology uses an exhaustive evaluation of all possible n -dimensional spaces (formed by n attributes) and angles to find an attribute τ that represents the global maximum correlation with the target petrophysical property. The total number of attribute spaces (N_s) to be evaluated in a MARS run is given by

$$N_s = \frac{N_A!}{N_D! \times (N_A - N_D)!}, \quad (3)$$

where N_A is the total number of elastic attributes to be used, and N_D is the dimension of the attribute spaces to be evaluated.

The final step in this workflow is to scale the attribute τ to units of the target property y :

$$y = m \times \tau + c, \quad (4)$$

where the coefficients m and c can be estimated by fitting a line between the attribute τ and the actual petrophysical property.

Case study 1: Barents Sea well 7120/12-2

Input data

Figure 2 shows the well log data used as an input for the MARS application. These data consist of both fundamental elastic properties (P-wave velocity V_P , S-wave velocity V_S , and density), and target petrophysical properties, e.g., water saturation S_w , total porosity ϕ_t , and clay volume V_{clay} logs. Because the final goal of MARS is to predict petrophysical properties using seismically derived elastic attributes, the first step consists of low-pass filtering the input well logs to approximate seismic resolution (black log curves in Figure 2).

Table 1. Example of a set of attributes used in a MARS run. Each number represents a single attribute, which is obtained after applying the mathematical operation shown in the leftmost column to the uppermost row. For example, the number 21 represents the attribute $1/\lambda\rho$. Because $I_S^2 = \mu\rho$ and $\sqrt{\mu\rho} = I_S$, these attributes have not been used in the analysis.

	I_P	I_S	$\frac{V_p}{V_s}$	$\lambda\rho$	$\mu\rho$	λ/μ	$(\lambda - \mu)\rho$	σ	$E\rho\rho$	$K\rho$	PDF
Attribute	1	7	12	18	24	29	35	41	47	47	59
$\ln(\text{Attribute})$	2	8	13	19	25	30	36	42	48	48	60
$e^{\text{Attribute}}$	3	9	14	20	26	31	37	43	49	49	61
$\frac{1}{\text{Attribute}}$	4	10	15	21	27	32	38	44	50	50	62
Attribute^2	5	—	16	22	28	33	38	45	51	51	63
$\sqrt{\text{Attribute}}$	6	11	17	23	—	34	40	46	52	52	64

Attribute computation

Any combination of elastic attributes that can be estimated independently from seismic inversion products and V_P , V_S , and density well logs can be used in the MARS analysis. Table 1 shows an example of a set of attributes that can be used in a MARS assessment. In this table, each number represents a single attribute, which is obtained after applying the mathematical op-

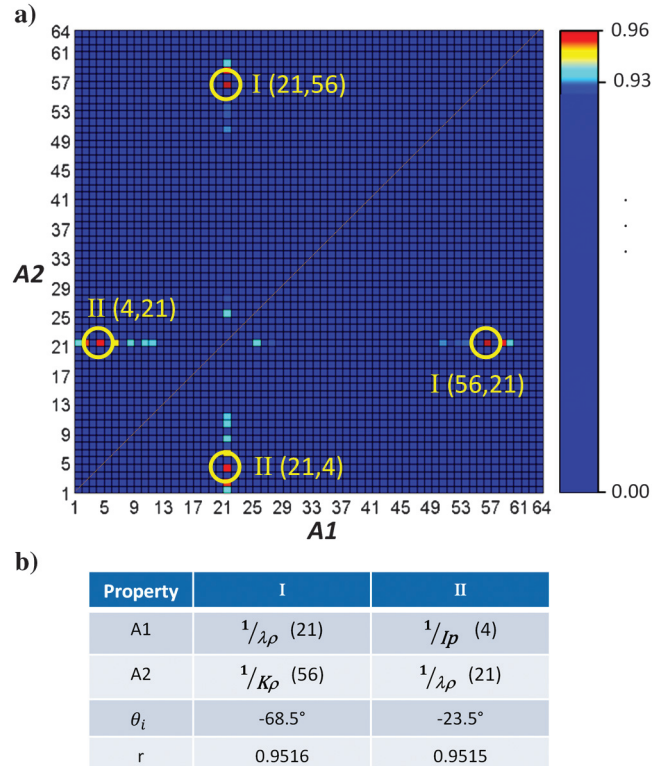


Figure 3. (a) Matrix showing the value of the correlation coefficient between the S_w log and the attribute τ , for each evaluated crossplot space. The row and column indexes represent the attributes specified in Table 1. Note that this is a symmetric matrix and the color map has been set to highlight the highest correlation coefficient values; i.e., all the values in the matrix less than 0.937 are shown in blue. (b) Attribute spaces and angles where the two highest correlations with the S_w log were found (I and II in Figure 3a).

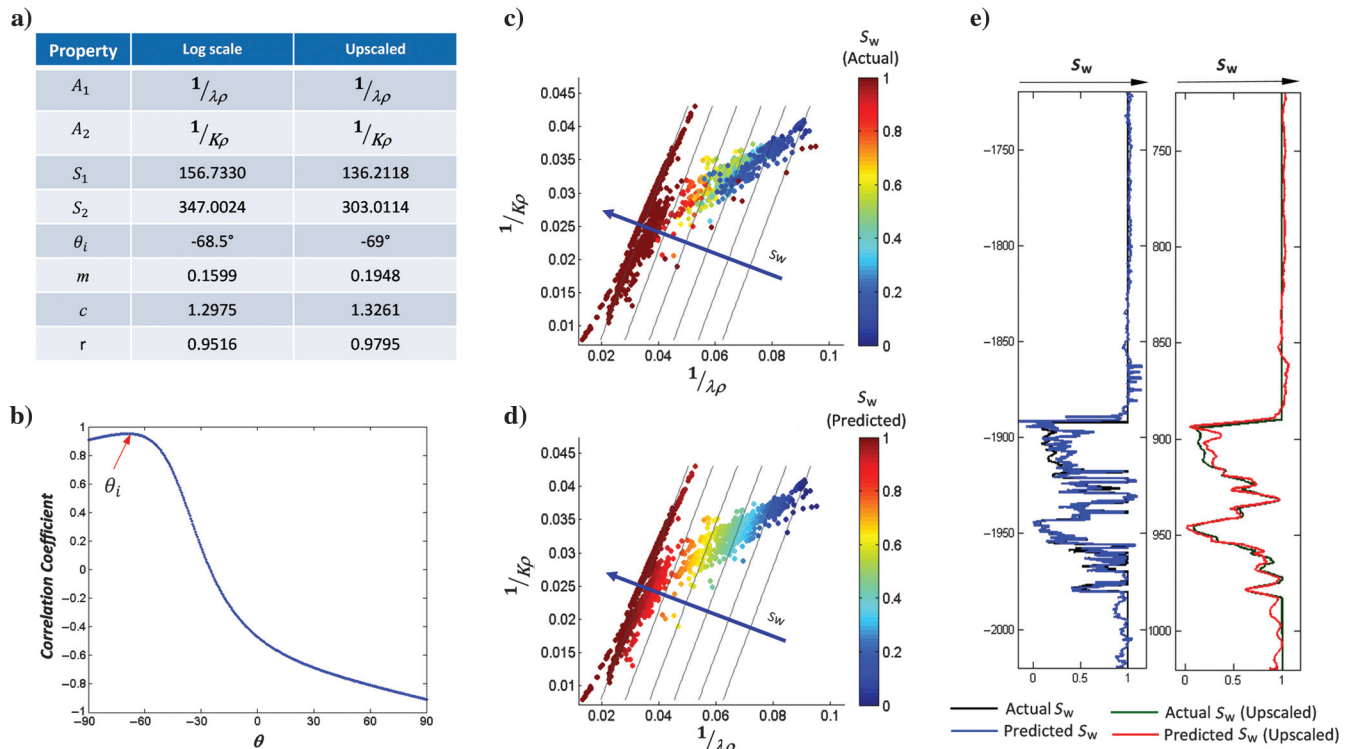


Figure 4. (a) Parameters used in equations 1 and 4 to estimate S_w from elastic attributes at original well-log scale and at the upscaled seismic resolution scale. This table also shows the correlation coefficient between the actual and predicted S_w logs. (b) Crossplot between θ versus the correlation coefficients between the S_w log and the set of attributes estimated via axis rotation, for the cases of the original well-log scale. (c and d) Comparison of the actual and predicted S_w log in the crossplot space $1/\lambda\rho$ versus $1/K\rho$. Blue arrows, orthogonal to the gray lines, indicate the maximum direction of change of S_w in this attribute space. (e) Comparison between the actual and predicted S_w logs for original and seismic resolution.

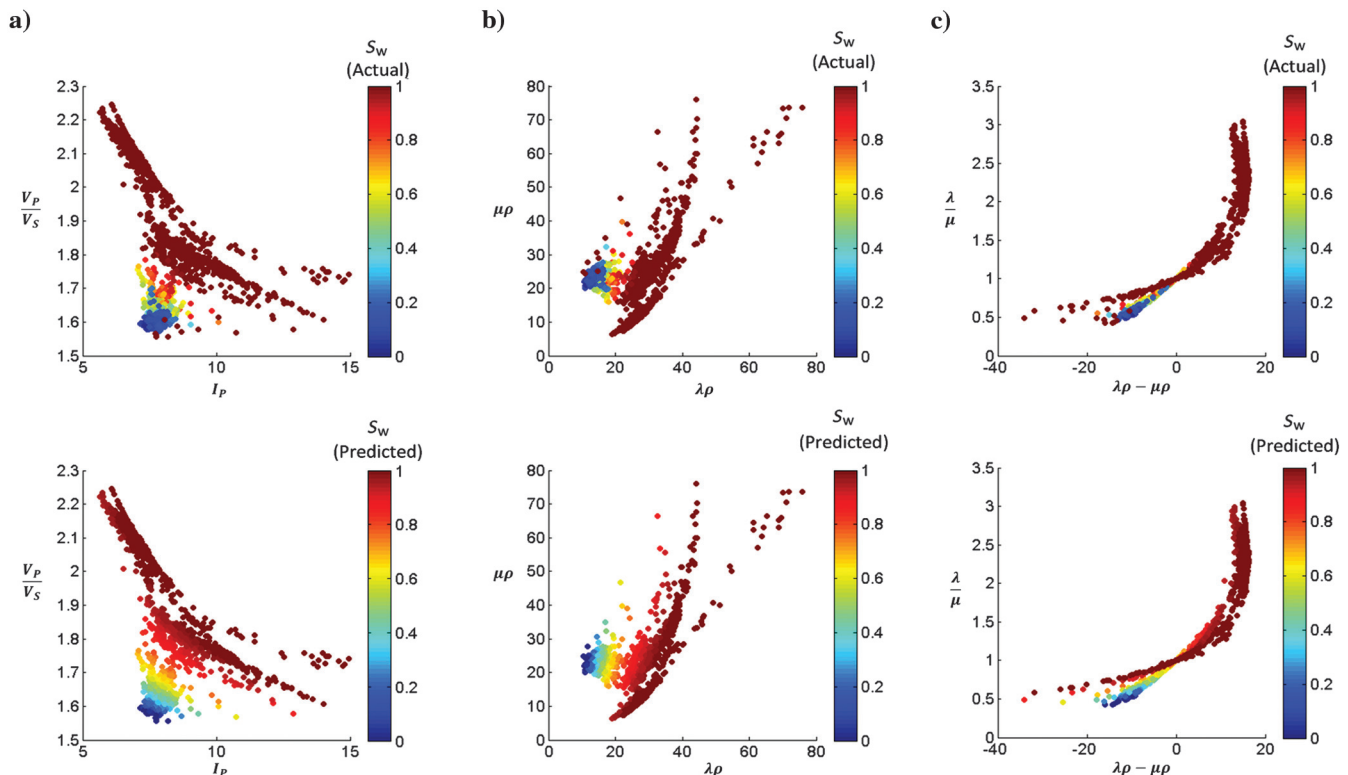


Figure 5. Comparison of the actual and predicted S_w in the attribute spaces: (a) V_p/V_s versus I_p , (b) $\lambda\rho$ versus $\mu\rho$, and (c) $\lambda\rho - \mu\rho$ versus λ/μ .

eration shown in the leftmost column to the elastic attribute shown in the uppermost row. For example, the number 21 represents the attribute $1/\lambda\rho$. The purpose of applying a mathematical operation (such as square root, power, inverse, logarithm, etc.) to attributes is to be able to model physical phenomena that exhibit nonlinear behavior. This is a mathematical strategy to linearize potential nonlinear relationship between the elastic attributes and the petrophysical properties, used with the goal of improving the correlation between the attribute τ and the target petrophysical property.

Water saturation estimation from two attributes

For the S_w estimation, MARS was run for a 2D combination of the 64 elastic attributes shown in Table 1, which can be derived from I_P and I_S , resulting in the evaluation of 2016 independent bidimensional spaces (see equation 3). Figure 3a shows a matrix with the absolute value of the highest correlation coefficient between the S_w log and the attribute τ , for each evaluated crossplot space. In this figure, the row and column indexes represent the attributes specified in Table 1. Note that this is a symmetric matrix, and the color map has been set to highlight the highest correlation coefficient values; i.e., all the values in the matrix less

than 0.937 are shown in blue. Even though MARS is a deterministic approach, the final solution is not unique; there are several crossplot spaces that can be used to create attributes with a high correlation to the target property. Figure 3b shows the attribute spaces (I and II) in which the two highest correlation values with the S_w log were found. In these attribute spaces, $1/\lambda\rho$ versus $1/K\rho$ and $1/I_P$ versus $1/\lambda\rho$, the correlation coefficient found with the S_w log was 0.9516 and 0.9515, respectively, which implies that either of these spaces can be equally used for the final application. Figure 4 shows the results obtained after running MARS and the comparison between the actual and predicted S_w logs. Figure 4a shows a table with the resultant parameters that were used in equations 1 and 3 to estimate an S_w log from elastic attributes. This table shows a comparison of the results obtained when original logs and upscaled logs are used. Although the estimated θ_i shows a small difference between the two cases, the m and c values differ more due to the difference in the dynamic range between the original and the up-scaled well-log data. Figure 4b shows a crossplot of θ versus the correlation coefficients between the derived set of attributes (estimated via axis rotation) and the S_w log; this shows a maximum correlation for $\theta = -68.5^\circ$. Figure 4c and 4d shows a comparison of the actual and

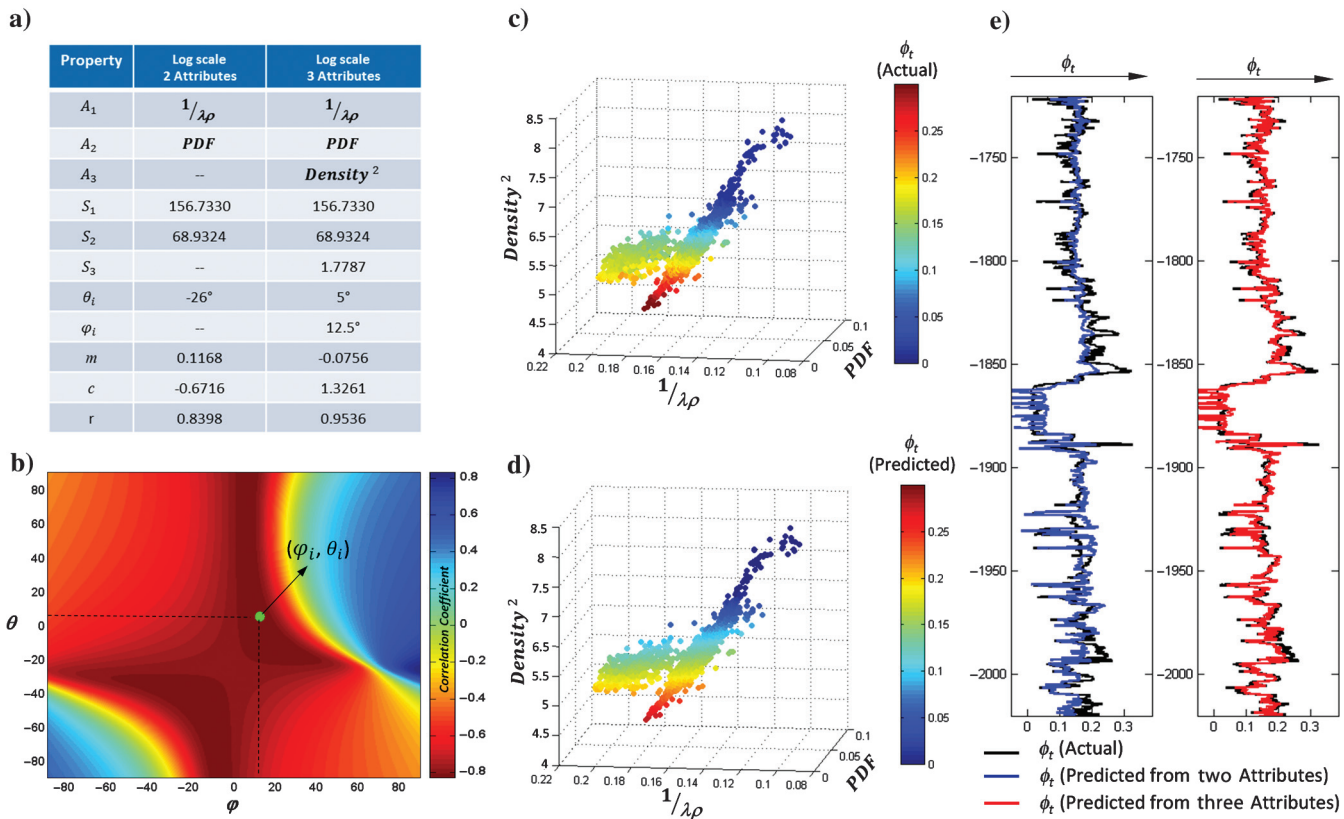


Figure 6. (a) Parameters used in equations 1, 2, and 4 to estimate ϕ_t from two and three attributes. This table also shows the correlation coefficient between the actual and predicted S_w logs. (b) Crossplot between θ and φ color coded by the correlation coefficients between ϕ_t and the set of attributes estimated via axis rotation. (c and d) Comparison of the actual and predicted ϕ_t log in the 3D space $1/\lambda\rho$ versus PDF versus ρ^2 . (e) Comparison between the actual and predicted ϕ_t logs.

predicted S_w logs in the $1/\lambda\rho$ versus $1/K\rho$ crossplot space. In these figures, the blue arrows that are orthogonal to the gray lines indicate the direction of

maximum change of S_w in this space. Figure 4e shows a comparison between the actual and predicted S_w logs for the log scale and upscaled cases. Note that the S_w

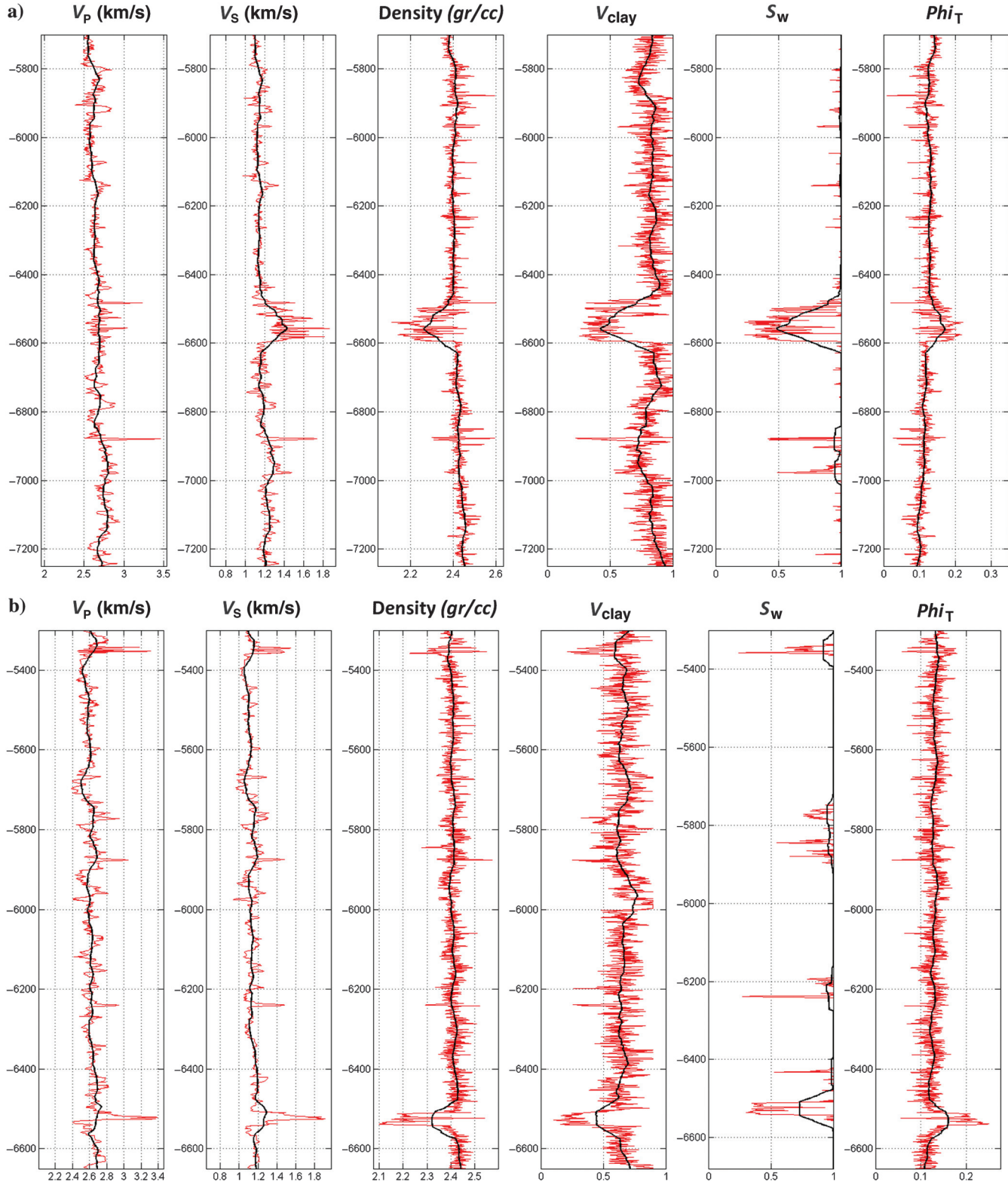


Figure 7. (a) Well-log information for well A. From left to right: V_p , V_s , density, V_{clay} , ϕ_t , and S_w . (b) Well-log information for well B. From left to right: V_p , V_s , density, V_{clay} , ϕ_t , and S_w . The red curves show the original logs, whereas the black curves show the upscaled versions to seismic resolution.

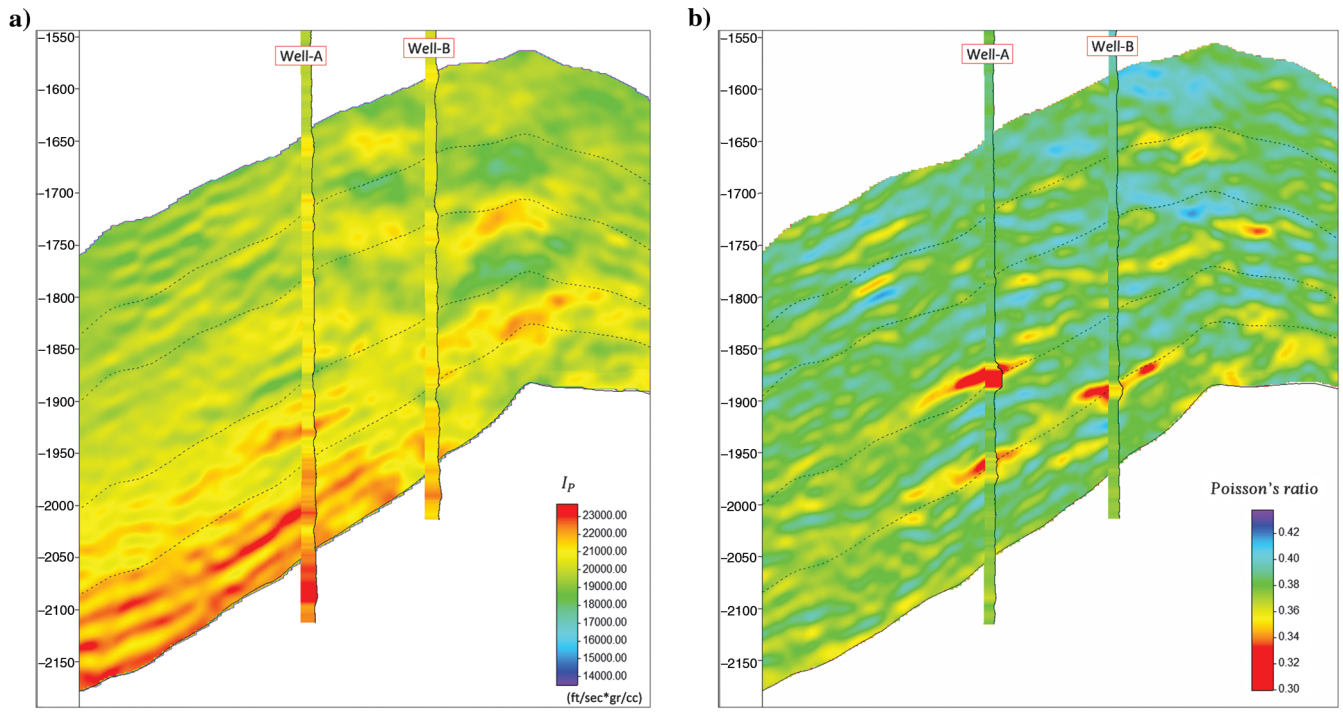


Figure 8. (a) Cross section through the I_P cube along wells A and B, together with the I_P logs (seismic scale). (b) Cross section through the Poisson's ratio cube along wells A and B, together with the Poisson's ratio logs (seismic scale). Notice the good match between the seismic and well-log-derived attributes.

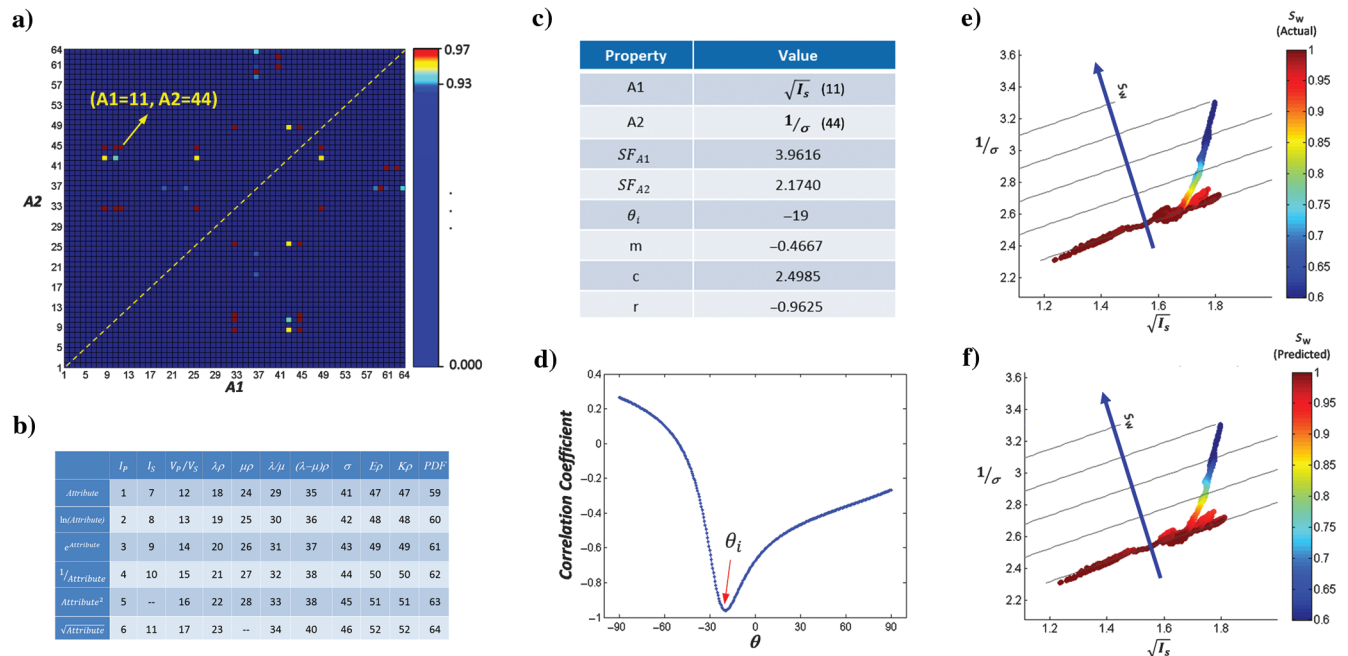


Figure 9. (a) Matrix showing the absolute value of the correlation coefficient between the S_w log and the attribute τ , for each evaluated crossplot space. Note that this is a symmetric matrix, and the colorbar has been set to highlight the highest correlation coefficient values. The global maximum correlation with S_w was found in the $\sqrt{I_s}$ versus $1/\sigma$ attribute space. (b) Set of attributes used in the MARS assessment. Each number represents a single attribute, which is obtained after applying the mathematical operation shown in the leftmost column to the uppermost row. (c) The resultant parameters obtained after running MARS in well A using upscaled well-log data. These parameters were used in equations 1 and 4 to estimate a S_w transform from elastic attributes. This table also shows the correlation coefficient between the actual and predicted S_w logs. (d) Crossplot between θ versus the correlation coefficients between S_w log and the set of attributes estimated via axis rotation. (e and f) Comparison of the actual and predicted S_w logs in the $1/\sigma$ versus $\sqrt{I_s}$ crossplot space.

curve is predicted very well in both cases using these two attributes. The upscaled results should be used to estimate a seismically derived S_w volume from seismically derived elastic attributes. On the other hand, some standard rock physics attributes spaces were used to compare the behavior of the actual and predicted S_w (Figure 5). Even though the property in question follows a nonlinear trend in most of these spaces in comparison with final domain used for the transform estimation (Figure 4c and 4d), trends of the predicted property match very well with the actual property. It demonstrates that the MARS technique worked effectively to solve the problem using linear equations.

Total porosity estimation from two and three attributes

For this case, it was assumed that a density attribute was available, which can be estimated from prestack seismic inversion if data from a wide aperture of reflection angles is available (Roy et al., 2006) and/or from prestack inversion of multicomponent seismic data (Garcia et al., 2010). Figure 6a shows a comparison of the final parameters obtained after applying MARS

in a 2D and 3D configuration. In the case of three attributes, two rotation angles have to be applied (see equation 2). Figure 6b shows a crossplot between angles θ and φ color coded by the correlation coefficients between ϕ_t and the set of attributes estimated via axis rotation. This plot is equivalent to the one shown in Figure 1b, but for the 3D case. Figure 6c and 6d shows a comparison of the actual and predicted ϕ_t logs in the 3D space defined by ρ^2 versus $1/\lambda\rho$ versus PDF. Figure 6e shows a comparison between the actual and predicted ϕ_t from two and three seismic attributes. The correlation coefficients between the attribute τ and ϕ_t increases from 0.8398 to 0.9536 when three attributes are used. The actual and estimated ϕ_t have a very good match for the three different lithologies that are present: sandstone, clay, and limestone.

Case study 2: Onshore Colombia

For this case study, MARS was used to estimate an S_w volume using a 2D approach in a mud-rich turbidite gas reservoir, of early and middle Miocene age, located onshore Colombia. The main reservoir consists of laminar, low-permeability sands in a thick shale-prone

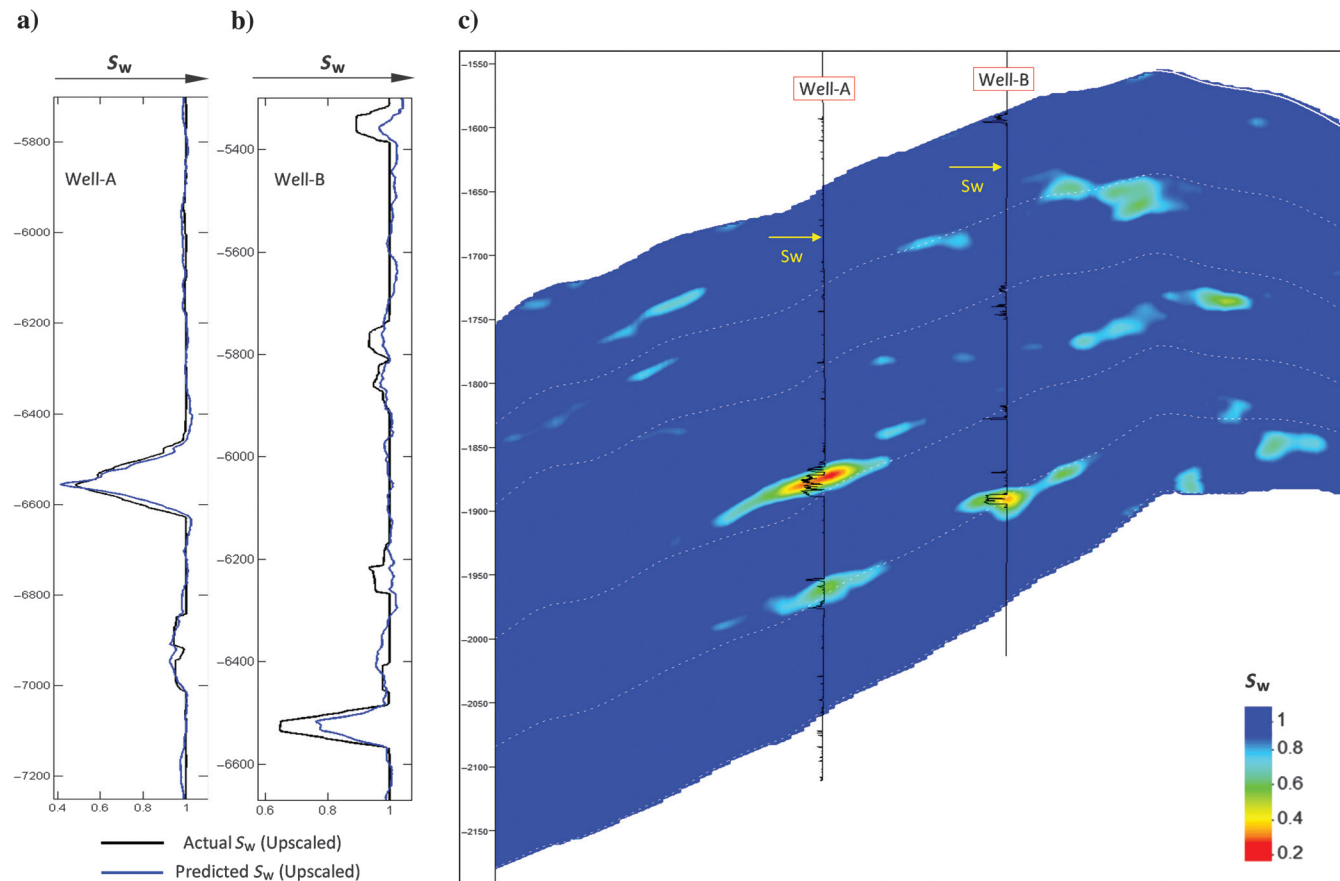


Figure 10. (a) For well A, comparison between the actual and predicted S_w logs upscaled to seismic resolution. (b) For well B (blind test), comparison between the actual and predicted S_w logs, upscaled to seismic resolution, estimated using the transform computed for well A. (c) Cross section along the resultant S_w volume along wells A and B (blind well) together with the S_w logs. Notice the good match between the seismic and well-log-derived S_w .

marine sequence, which was laid down in basin-floor conditions (Di Luca et al., 2014). Two wells (wells A and B) with a complete suite of high-quality measured elastic and petrophysical logs were available in the area (Figure 7), but only one of them (well A) was used in the analysis. The other well was used as a blind test of the MARS technique. Well-log and seismic gather conditioning followed by a prestack simultaneous seismic inversion were performed in the area (Alvarez et al., 2014), to obtain seismically derived volumes of I_P and I_S . Figure 8a and 8b shows cross sections through the resultant I_P and Poisson's ratio cube along wells A and B, together with its logs of I_P and Poisson's ratio upscaled to seismic resolution. Note the good match between the seismic and well-log-derived attributes. This is an important requirement for obtaining reliable reservoir property volumes from the MARS technique. Figure 9 shows the results obtained after running MARS on well A using upscaled log data. The global maximum correlation between the attribute τ and S_w was found in the attribute space $\sqrt{I_S}$ versus $1/\sigma$ at -19° , with a correlation of -0.9625 . Notice in Figure 9a, that in addition to this domain, several attribute spaces exhibited a very high correlation between τ and S_w , which implies that any of these spaces can be potentially used for the final application to the seismic data. Figure 9c shows the resultant parameters that were used in equations 1 and 4 to estimate an S_w transform from elastic attributes. Figures 9e, 9f, and 10a show a comparison between the actual and predicted S_w in the crossplot space $1/\sigma$ versus $\sqrt{I_S}$ and in the spatial domain, showing an excellent match between the actual S_w log, estimated though a petrophysical analysis and the S_w log estimated from elastic attributes using the MARS analysis. Next, as a quality-control step, the transform computed from well A was applied to the elastic properties measured at well B to compute S_w at well B. The result is shown in Figure 10b, in which there is a very good agreement between actual and predicted S_w logs. Finally, the resultant transform was applied to seismically derived volumes of $\sqrt{I_S}$ and $1/\sigma$ to obtain a volume of S_w . A cross section of the resultant S_w volume along wells A and B along with its S_w logs are shown in Figure 10c. In this figure, it is possible to see a good match between the seismic and well-log-derived S_w , not only at well A, which was used in the MARS assessment, but also at well B, which was used as a blind test location.

Conclusions

MARS is an accurate and robust method to predict petrophysical properties from elastic attributes using a numerical solution. For the case studies shown, customized transforms were found for the analyzed geologic setting to estimate reservoir properties from elastic attributes. The final goal of this workflow is the application of these transforms to seismically derived attributes to generate volumes of these properties; for this reason, the quality of the results also depends on the accuracy of

the seismic inversion products, which can be affected by the noise level of the seismic data. The resultant reservoir property volumes obtained from the MARS assessment can be used in production and exploration settings for reservoir characterization and delineation and as soft variables in geostatistical workflows for static model generation and reserve estimation.

Acknowledgments

We thank Pacific Rubiales Energy for allowing the use of their data and to present them in this article. In addition, we would like to thank L. MacGregor, G. Taylor, W. Marin, M. Suda, R. Ackermann, A. Pereira, and P. Williams for the stimulating discussions and for reviewing this manuscript. Finally, we would like to thanks the journal's reviewers and editors, especially to K. J. Marfurt.

References

- Alvarez, P., F. Bolivar, W. Marin, M. Di Luca, and T. Salinas, 2014, Seismic quantitative interpretation of a gas bearing reservoir — From rock physics to volumetric: 76th EAGE Conference and Exhibition, EAGE, Extended Abstracts, We P13 09.
- Connolly, P. A., 1999, Elastic impedance: The Leading Edge, **18**, 438–452, doi: [10.1190/1.1438307](https://doi.org/10.1190/1.1438307).
- Di Luca, M., T. Salinas, J. Arminio, G. Alvarez, P. Alvarez, F. Bolivar, and W. Marin, 2014, Seismic inversion and AVO analysis applied to predictive-modeling gas-condensate sands for exploration and early production in the Lower Magdalena Basin, Colombia: The Leading Edge, **33**, 746–756, doi: [10.1190/tle33070746.1](https://doi.org/10.1190/tle33070746.1).
- Garcia, G., J. Silva, F. Artola, E. Marquez, and J. Vanzeler, 2010, Enhanced density estimation from prestack inversion of multicomponent seismic data: The Leading Edge, **29**, 1220–1226, doi: [10.1190/1.3496912](https://doi.org/10.1190/1.3496912).
- Gonzalez, E. F., T. Mukerji, G. Mavko, and R. J. Michelena, 2003, Near and far offset P-to-S elastic impedance for discriminating fizz water from commercial gas: The Leading Edge, **22**, 1012–1015, doi: [10.1190/1.1623642](https://doi.org/10.1190/1.1623642).
- Goodway, B., T. Chen, and J. Downton, 1997, Improved AVO fluid detection and lithology discrimination using Lamé petrophysical parameters; “ $\lambda\rho$ ”, “ $\mu\rho$ ”, and “ λ/μ fluid stack”, from P- and S-inversions: 67th Annual International Meeting, SEG, Expanded Abstracts, 183–186.
- Mazumdar, P., 2007, Poisson dampening factor: The Leading Edge, **26**, 850–852, doi: [10.1190/1.2756862](https://doi.org/10.1190/1.2756862).
- Ødegaard, E., and P. Avseth, 2004, Well logs and seismic data analysis using rock physics templates: First Break, **22**, 37–43.
- Roy, B., P. Anno, and M. Gurch, 2006, Wide-angle inversion for density: Tests for heavy-oil reservoir characterization: 76th Annual International Meeting, SEG, Expanded Abstracts, 1660–1663.
- Whitcombe, D. N., P. A. Connolly, R. L. Reagan, and T. C. Redshaw, 2002, Extended elastic impedance for fluid

and lithology prediction: Geophysics, **67**, 63–67, doi: [10.1190/1.1451337](https://doi.org/10.1190/1.1451337).



Pedro Alvarez received a B.S. (2002) in geophysical engineering from the Universidad Central de Venezuela and an M.S. (2007) in petroleum geophysics from the Instituto Superior de la Energia/Heriot-Watt University. He worked for eight years as a seismic interpreter and reservoir geophysicist for PDVSA focusing in structural

and quantitative seismic interpretation of clastic and carbonate reservoirs. Since 2012, he has been working for Rock Solid Images, where he currently has the position of team lead/Sr. QI geoscientist. In this position, his main responsibility is the quantitative interpretation of post-stack, AVO, seismic inversion, and CSEM attributes using a geologic, geostatistical, and rock-physics framework. He has experience working in projects from Venezuela, Colombia, Mexico, USA, Australia, the Falkland Islands, the Middle East, and Norway. He is member of SEG, AAPG, and EAGE.



Francisco Bolívar received a B.S. (2007) in geophysical engineering from the Universidad Central de Venezuela and finished his postgraduate specialization in 2011 in oil and gas reservoir management. He joined Paradigm Geophysical in 2007, where he was part of the customer support consultants group in geosci-

ence. In 2008, he transferred to Tricon Geophysics Inc., where he was responsible of conduct seismic reservoir characterization services worldwide. During these years, he also taught numerical methods and seismic interpretation for the Geophysics Department of the Universidad Central de Venezuela. Here, he also advised some B.S. thesis work. In 2012, he joined Rock Solid Images as a seismic quantitative interpreter. Currently, he is the technical advisor for the seismic geoscientists group of that organization.

Mario Di Luca is a geophysicist with 12 years of experience in the oil and gas industry. He is currently involved in exploration and production projects in Colombia, with emphasis on seismic interpretation and geologic analysis. He has a keen interest in seismic attribute analysis applied to gas-bearing systems.



Trino Salinas G. received an M.S. (1997) in geophysics from the Colorado School of Mines and has around 30 years of work experience in petroleum seismology. He is a geophysicist specializing in seismic data processing, seismic inversion, AVO, and 4D analysis. He worked at Ecopetrol from 1989 to 2006 and at Saudi Aramco from 2006 to 2011. He is currently working at Pacific Rubiales Energy as part of the geoscience group.